Mass-related inversion symmetry breaking and phonon self-energy renormalization in isotopically labeled AB-stacked bilayer graphene

SCIENTIFIC REPORTS

OPEN

SUBJECT AREAS:
ELECTRONIC PROPERTIES AND DEVICES
MECHANICAL AND STRUCTURAL PROPERTIES AND DEVICES
SURFACES, INTERFACES AND THIN FILMS
SYNTHESIS OF GRAPHENE

Received
7 May 2013

Accepted
5 June 2013

Published
24 June 2013

Correspondence and requests for materials should be addressed to M.K. (kalbac@jh-inst.cas.cz) or P.T.A. (ptaraujo@mit.edu)

Mass-related inversion symmetry breaking and phonon self-energy renormalization in isotopically labeled AB-stacked bilayer graphene

Paulo T. Araujo[1], Otakar Frank[2], Daniela L. Mafra[1], Wenjing Fang[1], Jing Kong[1], Mildred S. Dresselhaus[1,3] & Martin Kalbac[1,2]

[1]Department of Electrical Engineering and Computer Science, MIT, Cambridge, Massachusetts 02139, USA, [2]J. Heyrovský Institute of Physical Chemistry, Academy of Sciences of the Czech Republic, v.v.i., Dolejškova 3, CZ-18223 Prague 8, Czech Republic, [3]Department of Physics, MIT, Cambridge, Massachusetts, 02139, USA.

A mass-related symmetry breaking in isotopically labeled bilayer graphene (2LG) was investigated during in-situ electrochemical charging of AB stacked (AB-2LG) and turbostratic (t-2LG) layers. The overlap of the two approaches, isotopic labeling and electronic doping, is powerful tool and allows to tailor, independently and distinctly, the thermal-related and transport-related phenomena in materials, since one can impose different symmetries for electrons and phonons in these systems. Variations in the system's phonon self-energy renormalizations due to the charge distribution and doping changes could be analyzed separately for each individual layer. Symmetry arguments together with first-order Raman spectra show that the single layer graphene (1LG), which is directly contacted to the electrode, has a higher concentration of charge carriers than the second graphene layer, which is not contacted by the electrode. These different charge distributions are reflected and demonstrated by different phonon self-energy renormalizations of the G modes for AB-2LG and for t-2LG.

Graphene, which is a gapless material, has gathered much attention due to its prospective fascinating applications. However, some of the proposed applications, such as transistor-based applications, cannot be realized in single layer graphene due to fundamental problems related to, for example, a creation of a band-gap. As an alternative, bilayer graphene (2LG) with AB stacked layers (AB-2LG) has different vibrational properties and also a different electronic structure than monolayer graphene (1LG) and might overcome some of the shortcomings of 1LG. For example, in AB-2LG it is possible to tune a bandgap by an external electric field, which enables realization of a field effect transistor with a tunable bandgap[1,2]. These potential advantages motivated several recent studies involving AB graphene[1,3–7].

Another challenge is the difficulty to address and probe individual layers in few layer graphene samples. This problem can be promptly solved by isotope labeling of individual layers, as has been recently demonstrated[8,9]. One can easily tune the frequency of the phonons by an exchange of the ^{12}C isotope with a ^{13}C isotope with essentially no change to the electronic structure. In this context, while isotopic labeling tunes the phonon properties (tuning, therefore, a gas of Bosons in the system), electronic doping provides an important tool to tune the electronic properties of graphene (tuning, therefore, a gas of Fermions in the system)[10–12]. It is important to note that, this approach tunes, distinctly and independently, the electronic and vibrational properties of the material. Indeed, by varying the ways one isotopic labels and/or electronic dopes the system, different symmetries can be achieved to describe phonons and electrons in the system, which allow us to control selection rules often important to describe several physics-related phenomena. As a consequence, we gain a powerful method to tailor the thermal-related and transport-related phenomena in the material.

The changes in the vibrational structure can be observed directly by Raman spectroscopy. The larger the amount of ^{13}C isotope that is introduced into the graphene layer, the lower the observed frequency of the Raman bands[8,9]. If the different layers in a few layer graphene sample contains different amount of ^{13}C isotope, one can distinguish their Raman bands in the isotopically doped spectra relative to that for the corresponding naturally occurring graphene layer containing only ^{12}C [9,13]. Also, the electronic doping can be realized by electrostatic

gating[1], electrochemical charging[10,11] or chemical doping[14,15] and several reports on charge-induced phenomena in 1LG are found in the literature for each of these doping methods. In few layer graphene (FLG) samples, the situation is more complex. Although the doping of 2LG[16,17] and FLG[18] has been reported, the results are difficult to interpret, since it is not clear how the doping charge is distributed in between the various graphene layers. This problem can be overcome for turbostratic 2LG (t-2LG), since a special 2LG sample can be prepared by sequential transfer of ^{12}C and ^{13}C graphene layers onto, for example, a SiO_2 substrate, so that the Raman features of the top and bottom layers could be resolved and analyzed separately[8]. In these samples one can determine the doping charge associated with each individual layer independently when both layers were similarly doped, as reported in Ref. 8. The experimental results from Ref. 8 suggested that the charge is distributed almost evenly between the top and bottom layers of 2LG when the two constituent layers are randomly stacked on a SiO_2 substrate.

As discussed above, the turbostratic FLG can be easily obtained by the subsequent deposition of ^{12}C and ^{13}C individual layers on the target substrate[8,9]. However, this procedure does not allow one to control the rotation angle between the graphene layers, and for this reason, it is not possible in this way to obtain AB-2LG. Recently, several studies of graphene add-layers (as grown in CVD methods) appeared[19–21]. These add-layers are additional graphene layers formed during the growth of a primary 1LG using a Cu catalyst and in many cases, AB stacked regions are observed for the add-layer relative to the continuous graphene layer. It has been shown that, even though the add-layers grow much slower than the primary 1LG, they continue to grow over the entire growth time[19]. Therefore, one can, by careful control of the isotope content of the CH_4 source and the reaction conditions, reach the situation where the top add-layer contains mostly one type of isotope (either ^{12}C or ^{13}C), while the continuous layer comprises the second type of isotope.

In the present study, we tuned the chemical vapor deposition (CVD) synthesis of the graphene bilayer to form AB stacked regions where the add-layer is synthesized from ^{13}C and the continuous layer (primary 1LG) is synthesized from the ^{12}C isotope, as shown in Fig. 1. In such a sample, we are able to address individual layers by Raman spectroscopy, follow the effect of phonon self-energy renormalizations for each individual layer separately and further understand how the interlayer (IL) interactions work in these isotopic systems.

Results

Raman spectra for the $^{12/13}C$ 2LG systems. The graphene samples were grown on a copper substrate and transferred to a SiO_2/Si substrate following the procedure in Ref. 21. During the growth, we changed the carbon isotope as follows: at the beginning of the growth we introduced $^{12}CH_4$ for 90 s. Next, we changed the carbon source to $^{13}CH_4$ and we continued the growth for 5 minutes more. Since the growth of the continuous layer is fast and the growth of the add-layer is slow[9], we obtained 2LG regions where a small central area is composed only from the ^{12}C isotope and the border area (about 70% of the sample) is composed of the ^{13}C isotope. The continuous layer that formed first is composed of the ^{12}C isotope[19]. Figure 1(a) shows a photograph of the resulting graphene sample obtained using an optical microscope after transfer of the so-called 2LG thus prepared onto a SiO_2/Si substrate. The hexagonal shaped darker region (delimited by the black dotted line) in Fig. 1(a) corresponds to the 2LG, while the rest of the area (the background area) of the imaged spot is covered by 1LG. Figure 1(b) shows a 2D Raman map plotting the G′(2D) spectral linewidth. The G′(2D) lineshape is very sensitive to the 2LG stacking order as well as to the isotopic composition of the layers[22]. In Fig. 1(b) it is possible to localize the ^{12}C 1LG, the $^{12/12}C$ AB-2LG as well as the $^{12/13}C$ AB-2LG.

Figure 2 shows a typical Raman spectrum of the 2LG inner region thus prepared in comparison to that of the ^{12}C 1LG outer region (note that the ^{12}C sample is expected to contain the natural isotopic abundance, which is 1.07% of ^{13}C). Figure 2 also shows the Raman spectrum for a standard CVD-derived ^{13}C 1LG. As expected for isotopic systems, the Raman spectrum of the ^{13}C 1LG sample exhibits the same Raman features as the Raman spectrum of the ^{12}C 1LG except for a downshift of all the Raman bands for the ^{13}C 1LG sample relative to the ^{12}C graphene sample[8]. The observed experimental downshifts of the D, the G and the G′ bands for the ^{13}C graphene with respect to those of the ^{12}C graphene are about 50 cm^{-1}, 60 cm^{-1} and 100 cm^{-1}, respectively[8]. In a continuum model, the frequency shifts of the Raman bands in the ^{13}C enriched material with respect to the ^{12}C counterpart originate from the increased mass of this isotope which is given by equation (1):

$$(\omega_0 - \omega)/\omega_0 = 1 - [(12 + c_0)/(12 + c)]^{1/2} \quad (1)$$

where ω_0 is the frequency of a particular Raman mode in the ^{12}C sample, $c = 0.99$ is the concentration of ^{13}C in the enriched sample,

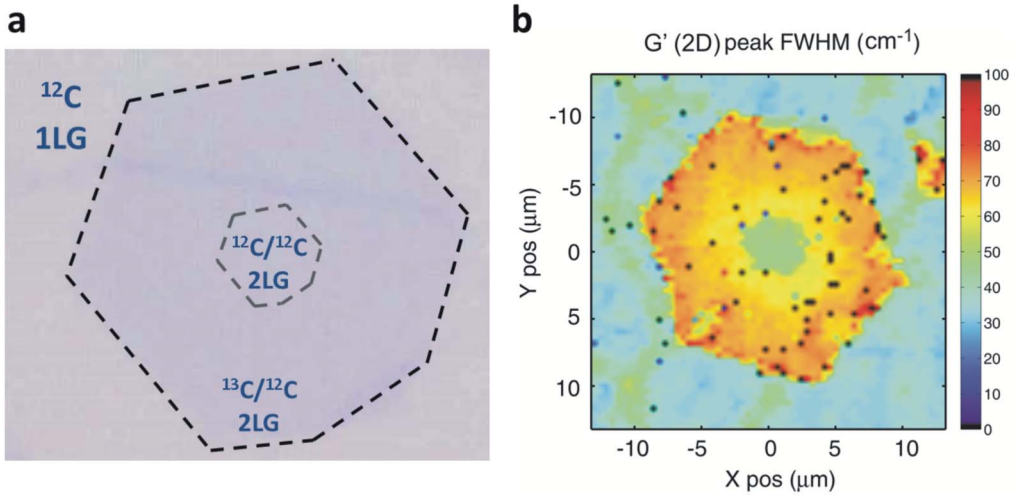

Figure 1 | Optical and spectroscopic images of the 2LG. (a) Optical image of the graphene with a ^{13}C-based add-layer (darker hexagonal area delimited by the dotted line) on the SiO_2/Si substrate. The diameter of the hexagon is about 10 μm. Note that the center (small area delimited by the gray dotted lines) of the add-layer forms a $^{12/12}C$ AB-2LG structure, while the remaining area is formed by $^{13/12}C$ AB-2LG. (b) G′ (2D) mode Full Width at Half Maximum (FWHM) indentifying the ^{12}C 1LG region (FWHM ~ 30 cm^{-1}), the $^{12/12}C$ AB-2LG region (FWHM ~ 45 cm^{-1}) and the $^{12/13}C$ AB-2LG region (FWHM ~ 75 cm^{-1}).

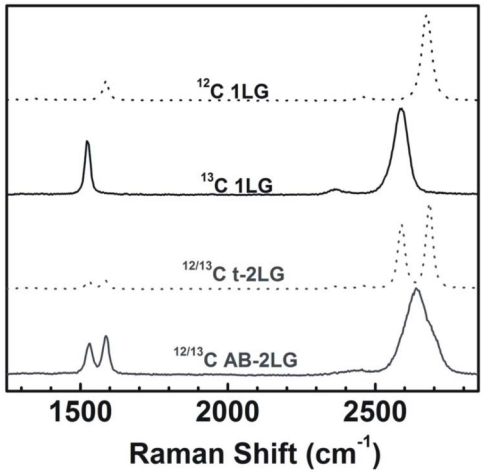

Figure 2 | Typical 1LG and 2LG Raman spectra. From the top to the bottom: typical Raman spectrum for the ^{12}C 1LG (black dotted line), typical Raman spectrum for the ^{13}C 1LG (black solid line), typical Raman spectrum for the $^{12/13}$C t-2LG (gray dotted line) and typical Raman spectrum for the $^{12/13}$C AB-2LG (gray solid line). The spectra are excited using 532 nm laser excitation energy.

and $c_0 = 0.0107$ is the natural abundance of ^{13}C in a typical ^{12}C sample. According to equation (1), the downshifts of the D, the G and the G′ bands are expected to be 48 cm^{-1}, 56 cm^{-1} and 95 cm^{-1}, respectively, which is in good agreement with our previous experimental results[8].

In the present work, we analyze the areas of the 2LG sample which comprise the initial ^{12}C 1LG and the ^{13}C regions of the add-layer composing this layered graphene ($^{12/13}$C 2LG). As expected (see Fig. 2), we observe two G modes in the Raman spectrum, one arising from the ^{12}C layer and the second arising from the ^{13}C layer. The as-grown peak positions of these G bands are at 1587 cm^{-1} and 1530 cm^{-1}, respectively. Interestingly, in the case of the G′ Raman mode, we obtained only a broad asymmetric band. This is in contrast to the situation in t-2LG prepared by the subsequent transfer of two separately grown graphene single layers[8]. In the latter case, the layers are misoriented and the phonons of different layers are fully independent since basically no IL interactions take place. In this case, we contemplate the same properties of the 1LG, which has 2 atoms per unit cell and 6 phonons modes. However, for the AB stacked samples, where the IL interactions are significant, one should also consider the interaction of the phonons to form, for example, the G′ mode. In short, when the IL interactions happen, the electronic structure of the AB-2LG departs from two non-interacting Dirac cones (related to the two non-interacting layers) around the K(K′)-point to become a hyperbolic electronic structure with two valence bands (π_1 and π_2) and two conduction bands (π_1* and π_2*). Regarding the phonon structure (and starting with the most known case), for a $^{12/12}$C AB-2LG we have 4 atoms per unit cell and 12 phonon modes. Thus, the G mode around the Γ-point will appear in two different peaks separated by 3 cm^{-1}, which has to do with the symmetric (S) E_g and antisymmetric (AS) E_u combinations involving the in-plane longitudinal optical (LO) and the in-plane tangential optical (iTO) modes of the top and bottom layers. Note that, while the S mode is Raman active, the AS is not, and therefore only one peak is seen in the G band region. For the G′ mode, which is a second-order process, in the case of the $^{12/12}$C AB-2LG we obtain 4 peaks due to the fact that iTO phonons can connect two different electronic states π_1*(π_2*) at the K-point with two possible π_1*(π_2*) states at the K′-point[23]. For the $^{12/13}$C t-2LG, each band can originate from either a ^{12}C or a ^{13}C graphene layer. Due to the different masses of the ^{12}C and ^{13}C atoms, these corresponding phonons observed in the ^{12}C and the ^{13}C graphene layers would differ in energy (frequency)[24].

For the $^{12/13}$C AB-2LG the situation is slightly different. Likewise the case of $^{12/12}$C AB-2LG, the unit cell of a $^{12/13}$C AB-2LG is composed of 4 atoms but now the atoms of the top layer are ^{12}C atoms while the atoms in the bottom layer are ^{13}C atoms. This has a very important symmetry consequence: because the ^{12}C and ^{13}C atoms have different masses, the unit cell for the $^{12/13}$C AB-2LG system has no inversion symmetry anymore for the phonons (note that for electrons the symmetry is kept) like is observed for the $^{12/12}$C AB-2LG system. Therefore, we have a mass-related symmetry breaking and the main consequence is that those S and AS modes discussed for $^{12/12}$C AB-2LG are no longer eigenstates of the system. Instead, the new eigenstates are now a mixing of the S and AS modes and the G mode region must comprise two Raman active peaks. A very similar effect happens when one applies an electric field in a $^{12/12}$C AB-2LG system[23]. However, in this case the inversion symmetry is broken for both electrons and phonons, so that we have a band gap opening in the K-point and, the S and AS modes are mixed and the G mode region has two Raman active peaks. Regarding the S and AS iTO phonon resonances, they are no longer unique around K(K′)-point, as is the case for the $^{12/12}$C AB-2LG. Due to the mass-related symmetry breaking, we now have two pairs of S and AS iTO mode resonances and the total number of bands contributing to the G′ mode would double giving eight Raman bands. The frequencies of each of these eight bands are close to each other, and therefore only one asymmetric broad band is observed experimentally in the Raman spectrum (Figure 2). It is worth mentioning that, due to its particular mechanism, this somewhat asymmetric G′ mode lineshape is a spectroscopic signature for the $^{12/13}$C AB-2LG systems[22].

Gate-modulated Raman spectroelectrochemistry. Next, we discuss the Raman spectroelectrochemistry results for the $^{12/13}$C AB-2LG systems. Figure 3 gives a schematic illustration of the experimental setup used here in which only the ^{12}C layer is connected to the electrode. Figure 4(b) shows the Raman spectra of $^{12/13}$C AB-2LG at different electrode potentials separated by 0.1 V. Interestingly, the behavior of the Raman spectra for $^{12/13}$C AB-2LG (Fig. 4(b)) is strongly different from that of $^{12/13}$C t-2LG (Fig. 4(a)). From now on, the following convention will be adopted: the Raman features in Figs. 4(a) and (b) both present two G modes; one with higher frequency, which is going to be called the HG mode and one with lower frequency, which is going to be called the LG mode. At first glance, especially in the positive potential regimes, one may identify some similarity between the potential dependent behavior of the HG modes for the $^{12/13}$C AB-2LG and t-2LG systems. However, the behavior of the LG mode for the $^{12/13}$C AB-2LG is completely

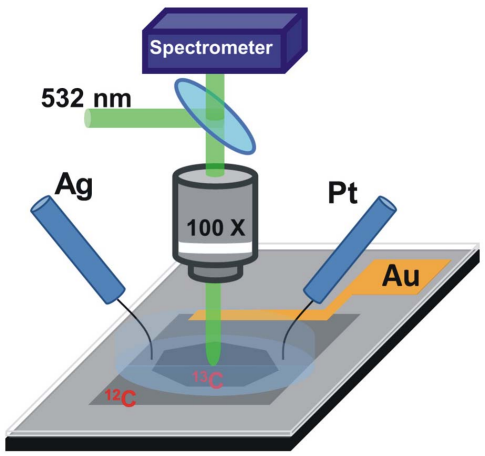

Figure 3 | *In-situ* Raman electrochemistry experimental configuration's scheme. Note that only the top ^{12}C layer is contacted in the current experimental configuration.

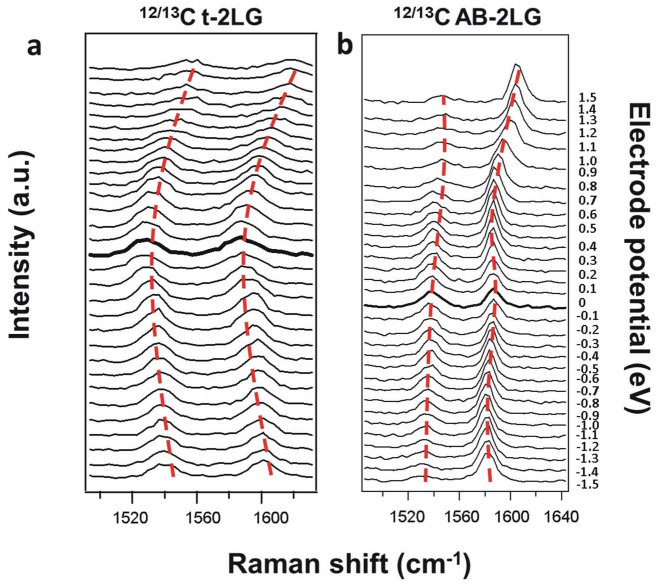

Figure 4 | Spectroelectrochemistry experiments. (a) *In-situ* Raman spectroelectrochemistry of the $^{12/13}$C t-2LG G modes and (b) *In-situ* Raman spectroelectrochemistry of the $^{12/13}$C AB-2LG G modes. The spectra are excited by 2.33 eV laser excitation energy and the electrode potentials range from −1.5 to 1.5 V vs. Ag/Ag$^+$ (from bottom to top) in units of 0.1 V. The red dashed curves are guide to eyes. Note that, due to electrochemistry conventions, positive potentials are filling the system with holes while negative potentials are filling the system with electrons.

different from both G mode lineshapes, that is, different from both the HG and LG modes of the $^{12/13}$C t-2LG. Namely, for the LG mode of the $^{12/13}$C AB-2LG, we observe small changes in the G mode frequency during negative doping. The LG mode downshifts from 1535 cm^{-1} to 1528 cm^{-1} going from 0 to −1.5 V. The corresponding frequency change in the LG mode of the $^{12/13}$C t-2LG (Fig. 4(a)) is much larger, and has an opposite direction: from 1528 cm^{-1} to 1546 cm^{-1}. For positive electrochemical potentials, we observe a larger change from 1535 cm^{-1} (at 0 V) to 1546 cm^{-1} (at 1.5 V) for the LG mode in AB-2LG, as seen in Fig. 4(b), but this frequency change is still smaller than in the case of the LG mode in t-2LG for which the change is from 1528 cm^{-1} (at 0 V) to 1563 cm^{-1} (at 1.5 V) as shown in Fig. 4(a).

In charged graphene, the frequency shift of the G mode, which is a first-order Raman mode around the Γ-point whose phonon momentum is null ($q = 0$), is related to both, the change in the C-C bond strength and the renormalization of the phonon self-energy associated with many-body effects[17]. Since for graphene a coupling between the lattice vibrations and the Dirac fermions is allowed (because the energy scales for the electron and phonon dynamics are comparable) the adiabatic Born-Oppenheimer approximation fails to describe phonons in graphene[24]. As a consequence, the interaction of the carriers in graphene with phonons must be included. These interactions cause electron-hole (e–h) pair creation (annihilation) due to phonon absorption (emission), with a lifetime related to the phonon linewidth (Γ), as observed in the Raman spectrum. This leads to a renormalization of the phonon energy, the phonon lifetime and consequently the energy of the carriers, that is, for both electrons and holes[25,26]. In charged graphene, every time we have a real creation (annihilation) of e–h pairs, which means that the phonon energy (E_{ph}) is bigger than $2|E_F|$ (E_F is the Fermi energy), a decrease of the G mode phonon frequency occurs. When E_F is moved away from the Dirac point, the formation of e–h pairs is eventually suppressed by the Pauli principle when the phonon energy (E_{ph}) is smaller than $2|E_F|$[24] resulting in a G mode frequency upshift for both negative and positive electrochemical potentials. It is worth mentioning that when $E_{ph} = 2|E_F|$, the so-called Kohn anomaly takes place and the maximum softening of the G mode frequency occurs[24].

Electrochemical doping is a reproducible and precise way to control the graphene doping, and we can easily evaluate the doping effects in graphene systems by monitoring the changes in the frequency of the Raman G mode during electrochemical charging[10,11]. To better elucidate the changes for both the LG and HG modes in the AB-2LG and t-2LG spectra, we analyzed the spectra in Figs. 4(a) and (b) with Voigt lineshapes. The fitting results are compiled in Fig. 5(a) (for both the LG and HG frequencies and linewidths of the $^{12/13}$C t-2LG) and Fig. 5(b) (for both the LG and HG frequencies and linewidths in $^{12/13}$C AB-2LG). First, we note that the frequency shifts of the LG and HG modes are observed to be smaller (for both, positive and negative potentials) for $^{12/13}$C AB-2LG with comparison to the $^{12/13}$C t-2LG. This suggests that different mechanisms are ruling the doping of $^{12/13}$C AB-2LG in comparison to the $^{12/13}$C t-2LG at the same applied electrode potential (which means the same charge concentration). Indeed, the t-2LG E_F will depend on n (n is the charge concentration) according to the following relation: $|E_{F(1LG)}| = \hbar|v_F|(\pi n)^{1/2}$ where v_F is the Fermi velocity, since the weakly interacting layers composing the t-2LG system keep the 1LG properties, while E_F for the AB-2LG will vary with n according to the following expression: $|E_{F(AB\text{-}2LG)}| = ½(-\gamma_1 + ((4\pi v_F^2 n)/3 + \gamma_1^2)^{1/2})$, where $\gamma_1 = 0.35$ eV. By inspecting both, $|E_{F(1LG)}|$ and $|E_{F(AB\text{-}2LG)}|$ relations, we see that, for a given change in n, E_F for the t-2LG changes more than the E_F for the AB-2LG[12,17]. Consequently, the frequency variations for the t-2LG G modes are expected to be larger than the frequency variations for the AB-2LG.

Besides the different charging of the layers in both, $^{12/13}$C AB-2LG and $^{12/13}$C t-2LG, which changes the magnitude of the phonon self-energy renormalizations, the observed experimental results for the G mode frequency and linewidth shifts are quite distinct for both samples, as observed in Figs. 5(a) and (b). Since the G mode occurs close to the Γ-point, in which the phonon wave vector magnitude q is negligible, the G mode is sensitive to each particular graphene layer. In other words, the G mode must reflect the charge associated to each particular layer. The behaviour observed for both the LG and HG modes for the $^{12/13}$C t-2LG (Figs. 4(a) and 5(a)) agrees well to the corresponding behavior observed for 1LG in which the frequency (linewidth) hardens (narrows) with increasing $|E_F|$. This behavior is already well understood and can be fully explained within the non-adiabatic phonon self-energy renormalizations[11,24]. Indeed, as expected for t-2LG systems, the results in Figs. 4(a) and 5(a) reflect that the two layers, ^{12}C and ^{13}C layers, are fully decoupled and the differences in the phonon renormalization magnitudes are due to different charging of each layer constituting the t-2LG. The renormalizations observed are related to E_g modes of each ^{13}C (the LG mode in Fig. 4(a)) and ^{12}C (the HG mode in Fig. 4(a)), separately. At this point, we must note that for the case of the $^{12/13}$C AB-2LG we do not observe the standard behavior expected for the dependence of the G mode as a function of E_F, in which the frequency (linewidth) hardens (narrows) with increasing $|E_F|$. For the $^{12/13}$C AB-2LG, on the other hand, in spite of the inhomogeneous charging of the ^{12}C and ^{13}C to be able to explain the different magnitudes for the frequency change, it cannot fully explain the results in Fig. 4(b) if we consider that the LG and HG modes are originating from the E_g modes from the top and bottom layers separately. Moreover, the results in Figs. 4(b) and 5(b) are also not fully consistent with other results observed for $^{12/12}$C AB-2LG available in the literature[16,27]. This inconsistence is expected since the phonon renormalizations strongly depend on the charge concentration of each of the layers in an AB-2LG.

In previous experiments both the top and bottom layers of the AB stacked 2LG were contacted by an electrode[16], and, for this reason, one can assume that E_F of both layers in the present case will be

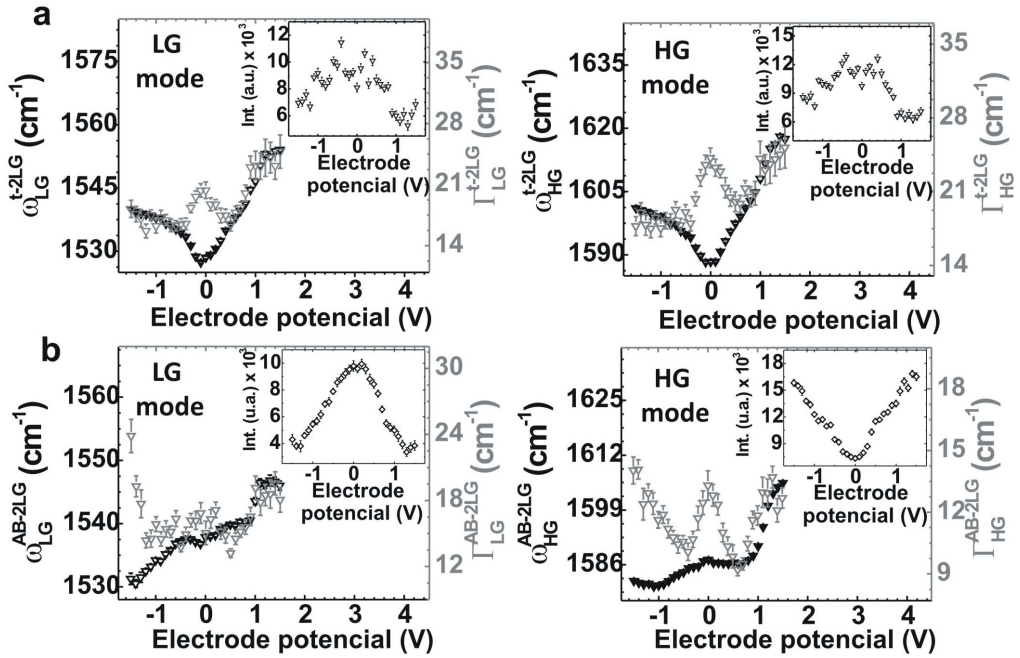

Figure 5 | Fitting analysis of the spectra showed in Fig. 4. (a) the frequency and linewidth behavior of the LG mode (left panel) and HG (right panel) in t-2LG as a function of the electrode potential. (b) the frequency and linewidth behavior of the LG mode (left panel) and HG (right panel) in AB-2LG as a function of the electrode potential. All insets present information on the intensity dependence with the electrode potential. Note that, due to electrochemistry conventions, positive potentials are filling the system with holes while negative potentials are filling the system with electrons.

equilibrated with each other thermodynamically (in other words, both layers are initially at the same potential). In our present work, the device is formed by the add-layer (the ^{13}C layer) which is located next to the continuous graphene layer, but only the continuous graphene layer is contacted to the electrode, as illustrated in Fig. 3 (in this situation the two layer are at two different potentials). In other words, the charge is transported by the ^{12}C layer to the $^{12/13}$C AB-2LG region. In our experimental setup, we must therefore consider a potential barrier due to the different position of E_F in the top layer relative to the bottom layer[1,28]. Therefore the doping of the ^{13}C graphene layer would depend on the efficiency of the charge transfer from the ^{12}C continuous layer to the ^{13}C add-layer. In addition, we should also consider the location of the add-layer with respect to the substrate, e.g., whether the ^{13}C layer is at the top or the bottom of the ^{12}C continuous layer. The injection of the charge carriers is more efficient to the top layer, which is closer to the electrolyte ions than to the bottom layer which is in contact with the substrate. In our case, the add-layer is at the bottom, as commonly expected for CVD-based 2LGs[29,30]. Therefore, this add-layer is electrically shielded by the top layer, and one can understand the latter observation, in which a smaller amount of charge is located on the add-layer. This is consistent with previous calculations by Das[17] and experiments by Fang *et al*[22]. We also note that a similar situation happens in the case of double wall carbon nanotubes where both outer and inner tubes are metallic and only the outer tube is contacted by the electrode[31]. The *in-situ* Raman spectroelectrochemical measurements on the latter samples also demonstrated that there is more charge located on the outer tube than on inner tube[31].

Discussion

In order to understand the results obtained here for the LG and HG modes in $^{12/13}$C AB-2LG, we must, as stated earlier in the text, recall that the unit cell for this systems has 4 atoms, as is the case for $^{12/12}$C AB-2LG, with the difference that the bottom atoms of the 2LG unit cell are ^{13}C atoms and the top atoms of the 2LG unit cell are ^{12}C atoms. In this case, the inversion symmetry in $^{12/13}$C AB-2LG is naturally broken due to the different ^{12}C and ^{13}C masses. As a result, what we are observing in Figs. 2 and 4(b) is, indeed, a S and AS mixing of the E_g and E_u modes distinctly observed only when the inversion symmetry exists, like is the case for $^{12/12}$C AB-2LG. This mixing of the E_g and E_u modes has also been observed for $^{12/12}$C AB-2LG when the latter is under the effect of an electric field[31]. Indeed, this mass-related symmetry breaking is confirmed by the electrochemistry measurements. As reported by Gava *et al.*[3] a signature of the E_g and E_u mixing is that the intensity ratio (I_{HG}/I_{LG}) between the HG (an anti-symmetric combination of E_g and E_u) and the LG modes (a symmetric combination of E_g and E_u) must increase with increasing $|E_F|$. This signature is confirmed by the experimental results, as shown in Fig. 6. Regarding the frequency, linewidth and intensity behavior of the two G band modes, Gava *et al.*[3] described their dependence in terms of the net 2LG charge concentration $n = n_{top} + n_{bottom}$. According to the charge concentration for the top (n_{top}) and bottom (n_{bottom}) layers, the frequency, linewidth and intensity can assume different behaviors[3]. Here, comparing the dependence of the HG and LG modes on potential voltage with the calculations performed in Ref. 3, we conclude that for the $^{12/13}$C AB-2LG, n_{bottom} (which is kept at constant potential) is positive (signifying an excess of electrons) and higher than the initial n_{top}. Note that to fully explain the frequency and linewidth behaviors, we still need to consider other effects such as the extinction of electron–hole (e–h) pair formation due to a band gap opening related to the application of an external electrical field and also the intraband related renormalizations of the phonon energies[32]. Both effects will be important for the positive voltages (which means excess of holes in the system) and negative voltages (which means excess of electrons in the system). Note that, due to conventions related to electrochemistry experiments, positive voltages means that the E_F is decreasing, so that holes are being injected to the system. On the other hand, negative voltages will mean that E_F is increasing, so that electrons are being injected to the system. This electrochemistry convention is opposite to the convention for back-gated experiments.

Next, based on the fact that $n_{bottom} > n_{top}$, we discuss the existence of an off-set in the change of the LG and HG mode frequencies in their dependence on electrode potential, as observed for the $^{12/13}$C

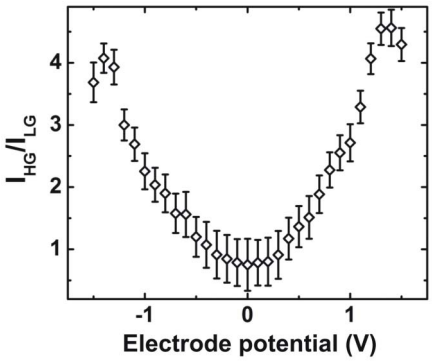

Figure 6 | Intensity ratio (I_{HG}/I_{LG}) between the LG and HG modes for the $^{12/13}$C AB-2LG as a function of the electrode potential. Note that I_{HG}/I_{LG}, which is a spectroscopic signature for the mixing of the E_g and E_u modes, increases with increasing electrode potential. Note that, due to electrochemistry conventions, positive potentials are filling the system with holes while negative potential are filling the system with electrons.

AB-2LG. This is, in particular, clear for the case of positive doping. As one can see from Fig. 4(b), there is a small increase in the frequency of the LG mode and almost no changes in the frequency of the HG mode up to an electrode potential of +1 V. Then, for the potentials above +1 V, the G mode frequencies are gradually increased and seem to saturate from the potential +1.3 V on. This behavior is in contrast to 1LG or t-2LG (Fig. 4a) where the frequency starts to change even at very low positive and negative applied potentials (±0.1 V). Besides the competition for the corrections in the phonon frequency between both phenomena, phonon self-energy renormalizations and changes in the chemical C-C bonds (excess of holes hardens the C-C bonds while excess of electrons softens the C-C bonds)[24], in AB-2LG, one should also consider subsequent filling (emptying) of the second electronic band in the conduction band π_2* (of the second electronic band in the valence band π_2) at higher electrode potentials. This band filling (emptying) is important to decide which phenomena will dominate and rule the frequency changes. In particular, it has been shown that the filling of π_2* may lead to a kink in the dependence of the Raman frequency on electrode potential[17] and this observation is consistent with a sudden change of the slope of the frequency/potential dependence ($\delta\omega_G/\delta V$) during hole doping (positive potentials) as seen in Fig. 4(b)[17]. Indeed, when E_F is at zero, real e–h pairs involving the π_1 and π_1* bands are being created all time, which contributes to decreasing the phonon frequency. At the same time, virtual e–h pairs are being created between π_1 and π_2 bands (in the valence band, which contributes to an increase in frequency) while no e–h pairs are being created between π_1* and π_2* in the conduction band. Note that, because it is a resonant effect, e–h pairs involving the π_1 and π_1* bands will dominate the virtual processes. Nothing is happening to the bonds since the system is not doped yet.

Let us now understand what happens when the system is doped with holes. In this case, when a first stage takes place (electrochemical potential between 0 and 1 V in Fig. 5(b)), the real e–h pair formation involving the bands π_1* and π_1 will be halted (since E_F is decreasing) and the e–h pairs involving the bands π_1 and π_2 will change their status from virtual to real e–h pairs. The net effect will be: the phonon self-energy renormalizations will decrease the frequency (broaden the linewidth), since the real e–h pair formation will favor the frequency changes, while the C-C bonds will harden hence increasing the frequency. On average, no (or a small) change in frequency is expected, in accordance with the observations. Precisely speaking, this competition between the phonon self-energy renormalizations versus C-C bond changes will certainly depend on the net charge density $n = n_{top} + n_{bottom}$ since this charge density will determine the E_F behavior in the system[33]. In our experiment, in which $n_{bottom} > n_{top}$, the explanations given so far explain well the behavior observed for the HG mode in the $^{12/13}$C AB-2LG but it cannot explain completely the behavior observed for the LG mode, whose frequency slightly increases in the potential range from 0 to 1 V (see Fig. 5(b)). To completely understand the LG mode, we need to consider a band gap opening, as discussed later in the text. Going further in the electrochemical potential, in a second stage, for electrochemical potentials larger than 1 V, the 2LG system is heavily doped with holes and then both, real and virtual e–h creations (annihilations) will be halted and the C-C bonds hardening will favor the frequency changes, resulting in a steep increase of the frequency[24].

When the 2LG system is doped with electrons, the virtual e–h pairs created (annihilated) due to phonon absorption (emission) involving the π_1 and π_2 bands will always exist, which contributes to increase the frequency. Again, in a first stage (electrochemical potential between −1 V and 0), a competition between real and virtual e–h pair formations involving the π_1 and π_1* bands and the π_1 and π_2 bands, respectively, will occur. When E_F continues to increase, eventually the e–h pair formations involving the π_1 and π_1* bands and the π_1 and π_2 bands will be virtual and real e–h pairs involving the π_1* and π_2* bands start occurring. The net consequence is that the real electron hole pair formation together with the softening of C-C bonds will be dominating (it is worth remembering that when the graphene systems are doped with electrons, the C-C bonds soften, which results in a decrease of phonon frequencies). The net result is a decrease in the frequency, as shown in Fig. 5(b). As we progress to the second stage (electrochemical potential <−1 V), all the e–h pair formations involving all the π_1, π_2, π_1* and π_2* will be virtual. However, this virtual e–h pair formation will be a small perturbation favored by the C-C bonds softening. The net effect is still a decrease in the phonon frequency. It is important to comment that the behaviors observed for the phonon linewidths are consistent with our explanations.

As mentioned, the explanations above do not fully explain the behavior of the LG mode for the $^{12/13}$C AB-2LG in the range from 0 to 1 V, which requires a band effect to be fully understood. In fact, since the graphene is on the substrate which is known to dope graphene, we can consider this situation as a device with a fixed voltage at the bottom gate and variable voltage at the top gate, which is realized by changing the applied electrode potential. The electrochemical doping method for varying E_F has generally been shown to be very efficient for the gating of devices[10]. Since we gradually increase the gate voltage in our experiment, the bandgap should be opened in the $^{12/13}$C AB-2LG electronic structure and, in principle, the charge carriers are no longer injected into the graphene sample, until E_F exceeds the band gap magnitude. We note that in contrast to previous studies, we used a potentiostat to control the potential of the gate electrode, and therefore the electric field is expected to be higher and the gap opening can be larger than the phonon energy. The gap opening should therefore be reflected in the Raman spectra of the doped AB-2LG. The situation can be analogous to a semiconducting SWCNT, where one can find an offset in doping which is equal to half the energy of the bandgap[34]. At this point, it is important to remember that since one of the layers is being kept at a constant potential, the opening of a band gap is accompanied by the respective change of E_F. This will make the band gap to be important at positive electrochemical voltages but unimportant for negative electrochemical voltages[35]. This is discussed as follows: the changes of the Raman G mode features are related to the creation (annihilation) of e–h pairs due to phonon absorption (emission) which hardens (narrows) the Raman band frequency (linewidth) and it is directly connected to the lifetime of the electron–hole pair, in other words, the average time spent by the phonon as an e–h pair. It is worth remembering that, the formation of e–h pairs can be prevented by the injection of charge carriers, to change E_F sufficiently so that energy and momentum can

no longer be conserved for e–h pair formation due to phonon absorption (emission). Indeed, we discussed that any time the condition $E_{ph} < 2|E_F|$ (E_{ph} stands for the phonon energy) is satisfied, the formation of real e–h pairs will be halted and as a consequence the G mode frequency will increase and the respective linewidth will decrease. Alternatively, the formation of real e–h pairs can be prevented by opening a bandgap, since the real e–h pair formation will be halted every time the band gap energy (E_{gap}) is larger than E_{ph} ($E_{ph} < E_{gap}$). In this case, any change in frequency will be more likely related to changes in the C-C bonds since they major any contribution involving virtual e–h pair creations related to the band-gap (precisely speaking, the formation of e–h pairs involving forbidden states of the bandgap, which can be understood as a virtual e–h pair creation as well, will be unlike since these e–h pairs involve forbidden states of the system). In other words, if the $E_{ph} > E_{gap}$ condition is satisfied, e–h pairs will be formed and the hardening (narrowing) of the G mode frequency (linewidth) should be observed independently of the E_{gap} value.

The bandgap opening, in fact, reflects spectral changes in the positive electrochemical potential values in the LG modes due to the applied gate potential, as shown in Fig. 5(b). Let us start analyzing the range of voltages from −1.5 to 0 V in Figs. 5(a) and (b). In Fig. 5(a), which shows the data for the $^{12/13}$C t-2LG, the frequency hardening followed by a saturation at around −1 V for the LG and HG modes is evident and means that the phonon self-energy renormalization is taking place and is a major effect between −1 V and 0 and from −1 V on, the doping-related changes in the C-C bonds, which decrease the phonon frequency, is a major effect. No band gap is introduced since the 2LG in question is turbostratic. Now, as shown in Fig. 5(b), the LG and HG frequencies decrease for the $^{12/13}$C AB-2LG, which means that the changes in the C-C bonds are the major changes, as explained above. For negative electrochemical potentials, in which electrons are being injected to the system, E_F will be in the conduction band before the condition $E_{ph} < E_{gap}$ occurs[35]. This means that the band gap will not play an important rule for negative potentials. For the range from 0 to +1 V, the frequency is roughly constant for the HG mode in Fig. 5(b) and slightly increases for the LG mode. This suggests that the band gap is likely affecting the LG mode which is halting the phonon renormalization, since when E_F decreases (meaning that the system is doped with holes) the electrons supposedly going from the π_1 band to the π_1* band will eventually fall into the band gap. During the time this happens, the C-C bond changes will be the major effect in the frequency changes (note that the frequency should increase according to Lazzeri *et al.*[24]). Additionally, we believe that the inhomogeneous charging of the top and bottom layers in AB-2LG could explain why the band gap almost does not affect the HG mode[17]. Finally, at high positive potentials above 1 V, the explanations given above are enough to explain the frequency changes since the gap will not affect the system anymore. Moreover, since the t-2LG system does not open a band gap, its frequency behavior (see Fig. 5(a)) with the electrochemical potential is totally explained within the phonon self-energy formalism and together with C-C bond changes.

In conclusion, we studied $^{12/13}$C AB-2LG by Raman spectroscopy and in situ Raman spectroelectrochemistry. A mass-related symmetry breaking is observed where the $^{12/13}$C AB-2LG exhibits two distinct G modes, one LG and another HG, which are related to a symmetric (LG) and anti-symmetric (HG) combination of E_g and E_u modes existing in the $^{12/12}$C AB-2LG, where no mass-related symmetry breaking takes place. Indeed, this mode mixing happens due to a mass-related symmetry breaking of the inversion symmetry usually present in the unit cell of AB-2LGs. In the case of $^{12/13}$C AB-2LG, this symmetry is naturally broken since the top atoms in the unit cell are ^{12}C atoms and the bottom atoms in the unit cell are ^{13}C atoms. This is different from $^{12/13}$C t-2LG, where the two distinct LG and HG modes are related to the E_g modes from the ^{13}C and ^{12}C individual layers, respectively. In $^{12/13}$C AB-2LG, the electrochemical charging reflects a smaller sensitivity of E_F to the electrode potential due to the effect of the modified electronic structure as compared to that for $^{12/13}$C t-2LG. In addition, spectroelectrochemical experiments in AB-2LG indicated more charge on the top layer than on the bottom layer.

Methods

Graphene flakes synthesis. The AB stacked 2LG was prepared using a modified CVD growth method. A thick copper foil (127 um thick, 99.9%, Alfa Aesar) forming an enclosure over the growth zone was used as a catalyst which was cleaned by dipping the copper into Ni etchant (Nitric acid, Transeneinc.) for 30 seconds. The growth procedure was as follows: the substrate was heated to 1000°C under 10 sccm H_2 for 30 min for annealing the substrate. Subsequently, the $^{12}CH_4$ was introduced for 90 sec, then the line was purged for 5 min using 100 sccmAr/10 sccm H_2, and finally $^{13}CH_4$ (99.5 atom%, Sigma-Aldrich) was introduced for 5 min.

Transfer procedure. To transfer the samples onto the SiO_2/Si substrate we used PMMA according to previously reported procedures[36]. In brief: Graphene on copper was coated with diluted 50:50 Poly(methyl methacrylate) (PMMA, 950 A9, Microchem, 4.5% in anisole) followed by removing the copper from the copper etchant (CE-100, Transene). Then the PMMA/graphene was washed by DI water to remove the residual copper etchant and the PMMA was removed by thermal annealing at 350°C for 3 h under a 200 sccm H_2/200 sccmAr atmosphere.

Electrochemistry Raman spectroscopy. For the doping experiments, the graphene samples on a SiO_2/Si substrate served as working electrodes and the samples were contacted using Au evaporated on a part of the substrate. The cell was completed with a Pt-counter electrode and an Ag-wire pseudo-reference electrode. The electrolyte solution used was 0.1 M $LiClO_4$ dissolved in dry propylenecarbonate/PMMA (Aldrich). Electrochemical doping of the working graphene electrode was carried out by varying the applied potential between −1.5 and 1.5 V vs. an Ag pseudoreference electrode (PAR potentiostat). We used a three electrode system and carried out measurements in the potentiostatic regime, so that no current was flowing through the reference electrode during the measurements. Care was also taken so that the current flow through the working electrode was minimal. Since the state (potential) of the pseudo-reference electrode is not changed during the measurement, the applied potential on the working electrode is well defined. The Raman spectra were excited by a Nd-YAG laser (Coherent). The spectrometer resolution was about 2.5 cm^{-1}. The spectrometer was interfaced to a microscope (Carl-Zeiss, objective 100×). The size of the laser spot was about 1 μm.

1. Castro, E. V. *et al.* Biased bilayer graphene: Semiconductor with a gap tunable by the electric field effect. *Phys. Rev. Lett.* **99**, 216802 (2007).
2. McCann, E. Asymmetry gap in the electronic band structure of bilayer graphene. *Phys. Rev. B* **74**, 161403 (2006).
3. Gava, P., Lazzeri, M., Saitta, A. & Mauri, F. Ab initio study of gap opening and screening effects in gated bilayer graphene. *Phys. Rev. B* **79**, 165431 (2009).
4. Malard, L. M., Elias, D. C., Alves, E. S. & Pimenta, M. A. Observation of Distinct Electron-Phonon Couplings in Gated Bilayer Graphene. *Phys. Rev. Lett.* **101**, 257401 (2008).
5. Oostinga, J. B., Heersche, H. B., Liu, X. L., Morpurgo, A. F. & Vandersypen, L. M. K. Gate-induced insulating state in bilayer graphene devices. *Nature Materials* **7**, 151–157 (2008).
6. Zhang, Y. B. *et al.* Direct observation of a widely tunable bandgap in bilayer graphene. *Nature* **459**, 820–823 (2009).
7. Weitz, R. T., Allen, M. T., Feldman, B. E., Martin, J. & Yacoby, A. Broken-Symmetry States in Doubly Gated Suspended Bilayer Graphene. *Science* **330**, 812–816 (2010).
8. Kalbac, M. *et al.* Raman spectroscopy and in situ Raman spectroelectrochemistry of bi-layer 12C/13C graphene. *Nano Letters* **11**, 1957–1963 (2011).
9. Kalbac, M., Kong, J. & Dresselhaus, M. S. Raman Spectroscopy as a Tool to Address Individual Graphene Layers in Few-Layer Graphene. *J. Phys. Chem. C* **116**, 19046–19050 (2012).
10. Kalbac, M. *et al.* The Influence of Strong Electron and Hole Doping on the Raman Intensity of Chemical Vapor-Deposition Graphene. *Acs Nano* **4**, 6055–6063 (2010).
11. Das, A. *et al.* Monitoring dopants by Raman scattering in an electrochemically top-gated graphene transistor. *Nat. Nanotechnol.* **3**, 210–215 (2008).
12. Yan, J., Zhang, Y. B., Kim, P. & Pinczuk, A. Electric field effect tuning of electron-phonon coupling in graphene. *Phys. Rev. Lett.* **98**, 166802 (2007).
13. Rodriguez-Nieva, J. F., Saito, R., Costa, S. D. & Dresselhaus, M. S. Effect of C-13 isotope doping on the optical phonon modes in graphene: Localization and Raman spectroscopy. *Phys. Rev. B* **85**, 245406 (2012).
14. Liu, H., Liu, Y. & Zhu, D. Chemical doping of graphene. *Journal of Materials Chemistry* **21**, 3335–3345 (2011).
15. Yu, W. J., Liao, L., Chae, S. H., Lee, Y. H. & Duan, X. Toward Tunable Band Gap and Tunable Dirac Point in Bilayer Graphene with Molecular Doping. *Nano Letters* **11**, 4759–4763 (2011).

16. Mafra, D. *et al.* Characterizing intrinsic charges in top gated bilayer graphene device by Raman spectroscopy. *Carbon* **50**, 3435–3439 (2012).
17. Das, A. *et al.* Phonon renormalization in doped bilayer graphene. *Phys. Rev. B* **79**, 155417 (2009).
18. Bruna, M. & Borini, S. Observation of Raman G-band splitting in top-doped few-layer graphene. *Phys. Rev. B* **81**, 125421 (2010).
19. Kalbac, M., Frank, O. & Kavan, L. The control of graphene double-layer formation in copper-catalyzed chemical vapor deposition. *Carbon* **50**, 3682–3687 (2012).
20. Nie, S. *et al.* Growth from below: bilayer graphene on copper by chemical vapor deposition. *New. J. Phys.* **14**, 093028 (2012).
21. Liu, L. *et al.* High-Yield Chemical Vapor Deposition Growth of High-Quality Large-Area AB-Stacked Bilayer Graphene. *Acs Nano* **6**, 8241–8249 (2012).
22. Fang, W. J. *et al.* Rapid Identification of Stacking Orientation in Isotopically Labeled Chemical-Vapor Grown Bilayer Graphene by Raman Spectroscopy. *Nano Letters* **13**, 1541–1548 (2013).
23. Thomsen, C. & Reich, S. Double resonant Raman scattering in graphite. *Phys. Rev. Lett.* **85**, 5214–5217 (2000).
24. Lazzeri, M. & Mauri, F. Nonadiabatic Kohn anomaly in a doped graphene monolayer. *Phys. Rev. Lett.* **97**, 266407 (2006).
25. Subramaniam, D. *et al.* Wave-Function Mapping of Graphene Quantum Dots with Soft Confinement. *Phys. Rev. Lett.* **108**, 046801 (2012).
26. Mafra, D. L. *et al.* Using gate-modulated Raman scattering and electron-phonon interactions to probe single-layer graphene: A different approach to assign phonon combination modes. *Phys. Rev. B* **86**, 195434 (2012).
27. Yan, J., Villarson, T., Henriksen, E. A., Kim, P. & Pinczuk, A. Optical phonon mixing in bilayer graphene with a broken inversion symmetry. *Phys. Rev. B* **80**, 241417 (2009).
28. Bandow, S. *et al.* Evidence for anomalously small charge transfer in doped single-wall carbon nanohorn aggregates with Li, K and Br. *Appl. Phys. A-Mater. Sci. Process.* **71**, 561–564 (2000).
29. Li, Q. & Chou, H. Growth of Adlayer Graphene on Cu Studied by Carbon Isotope Labeling. *Nano Letters* **13**, 486–490 (2013).
30. Wu, Y. P. *et al.* Growth Mechanism and Controlled Synthesis of AB-Stacked Bilayer Graphene on Cu-Ni Alloy Foils. *Acs Nano* **6**, 7731–7738 (2012).
31. Kalbac, M., Green, A. A., Hersam, M. C. & Kavan, L. Probing charge transfer between shells of double-walled carbon nanotubes sorted by outer-wall electronic type. *Chem.-Eur. J.* **17**, 9806–9815 (2011).
32. Das, A. & Sood, A. K. Renormalization of the phonon spectrum in semiconducting single-walled carbon nanotubes studied by Raman spectroscopy. *Phys. Rev. B* **79**, 235439 (2009).
33. Ando, T. & Koshino, M. Field Effects on Optical Phonons in Bilayer Graphene. *Journal of the Physical Society of Japan* **78**, 034709 (2009).
34. Kalbac, M. *et al.* Electrochemical charging of individual single-walled carbon nanotubes. *Acs Nano* **3**, 2320–2328 (2009).
35. Kuzmenko, A. B., Crassee, I., van der Marel, D., Blake, P. & Novoselov, K. S. Determination of the gate-tunable band gap and tight-binding parameters in bilayer graphene using infrared spectroscopy. *Phys. Rev. B* **80**, 165406 (2009).
36. Reina, A. *et al.* Large Area, Few-Layer Graphene Films on Arbitrary Substrates by Chemical Vapor Deposition. *Nano Letters* **9**, 30–35 (2009).

Acknowledgments

This work was supported by the Czech Ministry of Education, Youth and sports (LH-13022), and Czech Grant agency (P208-12-1062). The work done at MIT has been supported by NFS-DMR 10-04147. D.L.M. acknowledges the Brazilian agency CNPq.

Author contributions

M.K. performed measurements. P.T.A. and M.K. analyzed and explained the data. P.T.A. and M.K. wrote the manuscript. O.F., D.L.M., W.F., J.K. and M.S.D. discussed and reviewed the manuscript contents.

Additional information

Competing financial interests: The authors declare no competing financial interests.

How to cite this article: Araujo, P.T. *et al.* Mass-related inversion symmetry breaking and phonon self-energy renormalization in isotopically labeled AB-stacked bilayer graphene. *Sci. Rep.* **3**, 2061; DOI:10.1038/srep02061 (2013).